Ultrafast shift and rectification photocurrents in GaAs quantum wells: Excitation intensity dependence and the importance of band mixing

Huynh Thanh Duc,[1,2] Reinold Podzimski,[1] Shekhar Priyadarshi,[3] Mark Bieler,[3] and Torsten Meier[1]

[1]*Department of Physics and CeOPP, Universität Paderborn, Warburger Strasse 100, D-33098 Paderborn, Germany*
[2]*Ho Chi Minh City Institute of Physics, Vietnam Academy of Science and Technology, Mac Dinh Chi Str. 1, District 1, Ho Chi Minh City, Vietnam*
[3]*Physikalisch-Technische Bundesanstalt, Bundesallee 100, D-38116 Braunschweig, Germany*

A microscopic approach that is based on the multisubband semiconductor Bloch equations formulated in the basis of a 14-band $\mathbf{k} \cdot \mathbf{p}$ model is employed to compute the temporal dynamics of photocurrents in GaAs quantum wells following excitation with femtosecond laser pulses. This approach provides a transparent description of the interband, intersubband, and intraband excitations, fully includes all resonant as well as off-resonant excitations, and treats the light-matter interaction nonperturbatively. For linearly polarized excitations, the photocurrents contain contributions from shift and rectification currents. We numerically compute and analyze these currents generated by excitation with femtosecond laser pulses for [110]- and [111]-oriented GaAs quantum wells. It is shown that the often employed perturbative $\chi^{(2)}$ approach breaks down for peak fields larger than about 10 kV/cm, and that nonperturbative effects lead to a reduction of the peak values of the shift and rectification currents and to temporal oscillations that originate from Rabi flopping. In particular, we find a complex oscillatory photon energy dependence of the magnitudes of the shift and rectification currents. Our simulations demonstrate that this dependence is the result of mixing between the heavy- and light-hole valence bands. This is a surprising finding since the band mixing has an even larger influence on the strength of the photocurrents than the absorption coefficient. For [110]-oriented GaAs quantum wells, the calculated photon energy dependence is compared to experimental results, and good agreement is obtained. This validates our theoretical approach.

I. INTRODUCTION

In systems of sufficiently reduced symmetry, it is possible to generate electrical currents on ultrafast time scales without any applied bias simply by the optical excitation with suitable laser pulses. In particular, in noncentrosymmetric semiconductor systems, the nonvanishing second-order optical susceptibility $\chi^{(2)}$ allows one to generate photocurrents by excitation with a single optical pulse [1–24]. As was shown by Sipe *et al.* [6], $\chi^{(2)}$ contains three different contributions that correspond to three kinds of photocurrent, namely injection, shift, and rectification currents. Injection currents are caused by asymmetric populations of spin-polarized carriers in k space that originate from Dresselhaus and/or Rashba spin splittings in systems of sufficiently reduced symmetry. To excite spin-polarized carriers, circularly polarized light fields are required. Without any additional electric or magnetic fields, injection currents do not exist in bulk GaAs. They are, however, present in GaAs quantum wells (QW) with lower symmetry [10,19,20].

Under the action of an optical field that induces interband transitions, the electronic charge density in the noncentrosymmetric GaAs crystal is shifted in real space from the As atoms toward the neighboring Ga atoms, and this process leads to the so-called shift current [15]. Additionally, the spatial shift of bound electrons leads to a static polarization, i.e., optical rectification. If the optical rectification is time-varying, e.g., due to the time dependence of the optical pulse envelope, it induces another kind of current: the rectification current. Unlike injection currents, which are created by resonantly excited carriers, and shift currents, which require a resonant excitation in first order and therefore exist for excitation frequencies above the band gap, rectification currents are present for all photon energies.

Previously, we have developed a microscopic approach [20] in which we employed the commonly used 14-band $\mathbf{k} \cdot \mathbf{p}$ method to obtain the electron band structure and the Bloch functions for GaAs QWs, and we used the wave functions to formulate the multiband semiconductor Bloch equations (SBE). We solved the SBE to describe the optoelectronic response excited by ultrashort laser pulses. Using this approach, we analyzed injection currents generated by circularly polarized pulses in GaAs QWs, and we obtained results in quantitative agreement with experiment [19]. When limiting our approach to a perturbative analysis, we were able to reproduce the magnitude and the dynamics of the GaAs shift current obtained in Ref. [15], where on the basis of a full *ab initio* band structure, a second-order ($\chi^{(2)}$) analysis of the optical response was performed.

Here, we extend our approach to describe, in addition to injection and shift currents, also rectification currents. Thus we are able to describe all three photocurrents that exist in the second-order response of noncentrosymmetric semiconductors [6] in a unified way directly in the time domain and nonperturbatively in the light-matter interaction. We would like to point out that (unlike the case of injection currents) due to the involved nonresonant excitations to higher bands, the rotating-wave approximation cannot be applied for simulations of shift and rectification currents in the framework of Bloch equations, which significantly increases the numerical effort. We apply our microscopic approach to analyze shift and rectification currents in GaAs QW systems. It is shown that for large enough excitation intensities, nonperturbative effects arising from Pauli blocking lead to a reduction of the peak values of the shift and rectification currents and to intensity-dependent temporal oscillations, which originate from Rabi

flopping. The magnitude and direction of the photocurrents depend on the polarization direction of the incident pulse, and the strength of different intra- and intersubband coherences to the currents depends strongly on the excitation geometry. Furthermore, we find an oscillatory dependence of the currents on the photon energy, which is also confirmed experimentally. Our simulations demonstrate that this dependence is caused by valence-band mixing. This is an interesting finding since it emphasizes the tremendous influence of band mixing on transport phenomena, and it might be the beginning of new applications. To keep the numerical requirements within reasonable limits, excitonic effects are neglected in our present calculations.

This paper is organized as follows. In Sec. II, we present our theoretical approach. In Sec. III, several numerical results for shift and rectification currents in [110]- and [111]-oriented QWs are discussed. Experimental results and a comparison between experiment and theory are shown in Sec. IV. Finally, the main results are summarized briefly in Sec. V.

II. THEORETICAL APPROACH

The energies and wave functions of electrons in a semiconductor QW are described by the Schrödinger equation

$$\left[\frac{\hbar^2}{2m_0}\nabla^2 + V_0 + H_{\text{SO}} + V_{\text{conf}}\right]\psi = \varepsilon\psi, \quad (1)$$

where V_0 is the periodic lattice potential, H_{SO} is the spin-orbit interaction, and V_{conf} is the confinement potential. To obtain a realistic electronic band structure and wave functions near the Γ-point, we employ a 14-band $\mathbf{k} \cdot \mathbf{p}$ method [25–27] within the envelope function approximation. By choosing the z axis as the growth direction of the QW and writing the electron wave function as $\psi = e^{i\mathbf{k}_\parallel \cdot \mathbf{r}_\parallel} \sum_{n=1}^{14} f_{\mathbf{k}_\parallel}^n(z) u_n$, where $\mathbf{k}_\parallel = (k_x, k_y)$ is the in-plane wave vector, u_n are band-edge Bloch functions, and $f_{\mathbf{k}_\parallel}^n$ are slowly varying envelope functions, Eq. (1) becomes

$$\sum_{m=1}^{14}\left[H_{nm}^{\mathbf{k}\cdot\mathbf{p}}(\hat{\mathbf{k}}) + V_n(z)\delta_{nm}\right]f_{\mathbf{k}_\parallel}^m(z) = \varepsilon_{\mathbf{k}_\parallel} f_{\mathbf{k}_\parallel}^n(z), \quad (2)$$

where $H_{nm}^{\mathbf{k}\cdot\mathbf{p}}$ are the matrix elements of the 14-band $\mathbf{k} \cdot \mathbf{p}$ Hamiltonian with $\hat{\mathbf{k}} = (k_x, k_y, -i\partial/\partial z)$, and $V_n(z)$ is the band-offset potential of the well, which is taken to be centered at $z = 0$. To solve Eq. (2), we expand the envelope function into plane waves [27] $f_{\mathbf{k}_\parallel}^n(z) = \sum_{j=1}^{N} c_{n\mathbf{k}_\parallel}^j \phi_j(z)$, where $\phi_j(z) = \sqrt{\frac{2}{L}} \sin\left[\frac{\pi j}{L}(z + \frac{L}{2})\right]$ for $-L/2 \leqslant z \leqslant L/2$ and $\phi_j(z) = 0$ otherwise. This leads to a $14N \times 14N$ eigenvalue equation. By numerical diagonalizations of the matrix for several values of $\mathbf{k}_\parallel$, the electronic band structure is obtained. The number of plane-wave functions N and the width L are chosen to ensure convergence of the results.

To analyze the dynamics of photoexcited semiconductor QWs, we use a Hamiltonian that contains the band structure and the light-matter interaction in velocity gauge,

$$H = \sum_{\lambda, \mathbf{k}_\parallel} \varepsilon_{\lambda\mathbf{k}_\parallel} a_{\lambda\mathbf{k}_\parallel}^\dagger a_{\lambda\mathbf{k}_\parallel} + e\mathbf{A}(t) \cdot \sum_{\lambda, \lambda', \mathbf{k}_\parallel} \mathbf{v}_{\lambda\lambda'\mathbf{k}_\parallel} a_{\lambda\mathbf{k}_\parallel}^\dagger a_{\lambda'\mathbf{k}_\parallel}, \quad (3)$$

where $\varepsilon_{\lambda\mathbf{k}_\parallel}$ is the energy and $a_{\lambda\mathbf{k}_\parallel}^\dagger$ ($a_{\lambda\mathbf{k}_\parallel}$) is the creation (annihilation) operator of an electron in band λ with wave vector $\mathbf{k}_\parallel$, $\mathbf{A}(t)$ is the vector potential of the light field, and $\mathbf{v}_{\lambda\lambda'\mathbf{k}_\parallel}$ is the velocity matrix element between Bloch states,

$$\mathbf{v}_{\lambda\lambda'\mathbf{k}_\parallel} = \frac{1}{\hbar} \sum_{n,m=1}^{14} \int dz \, f_{\lambda\mathbf{k}_\parallel}^{n*} (\nabla_{\mathbf{k}} H^{\mathbf{k}\cdot\mathbf{p}})_{nm} f_{\lambda'\mathbf{k}_\parallel}^m. \quad (4)$$

From the Heisenberg equation of motion, we obtain the well-known multiband SBE [20,28,29], which describes the time evolution of the microscopic interband and intersubband polarizations $p_{\lambda\lambda'\mathbf{k}_\parallel} = \langle a_{\lambda\mathbf{k}_\parallel}^\dagger a_{\lambda'\mathbf{k}_\parallel}\rangle$ with $\lambda \neq \lambda'$ and the electron occupations $n_{\lambda\mathbf{k}_\parallel} = \langle a_{\lambda\mathbf{k}_\parallel}^\dagger a_{\lambda\mathbf{k}_\parallel}\rangle$,

$$\frac{\partial}{\partial t} p_{\lambda\lambda'\mathbf{k}_\parallel}(t) = i(\omega_{\lambda\lambda'\mathbf{k}_\parallel} + i/\tau_2)\, p_{\lambda\lambda'\mathbf{k}_\parallel}$$
$$+ \frac{i}{\hbar} e\mathbf{A}(t) \cdot \mathbf{v}_{\lambda'\lambda\mathbf{k}_\parallel}(n_{\lambda'\mathbf{k}_\parallel} - n_{\lambda\mathbf{k}_\parallel})$$
$$+ \frac{i}{\hbar} e\mathbf{A}(t) \cdot \left[\sum_{\nu \neq \lambda'} \mathbf{v}_{\nu\lambda\mathbf{k}_\parallel} p_{\nu\lambda'\mathbf{k}_\parallel} - \sum_{\nu \neq \lambda} \mathbf{v}_{\lambda'\nu\mathbf{k}_\parallel} p_{\lambda\nu\mathbf{k}_\parallel}\right], \quad (5)$$

$$\frac{\partial}{\partial t} n_{\lambda\mathbf{k}_\parallel}(t) = -\frac{2}{\hbar} \text{Im}\left[e\mathbf{A}(t) \cdot \sum_{\lambda' \neq \lambda} \mathbf{v}_{\lambda'\lambda\mathbf{k}_\parallel} p_{\lambda'\lambda\mathbf{k}_\parallel}\right]$$
$$- \frac{1}{\tau_1}\left(n_{\lambda\mathbf{k}_\parallel} - n_{\lambda\mathbf{k}_\parallel}^{\text{eq}}(n,T)\right), \quad (6)$$

where $\omega_{\lambda\lambda'\mathbf{k}_\parallel} = (\varepsilon_{\lambda\mathbf{k}_\parallel} - \varepsilon_{\lambda'\mathbf{k}_\parallel})/\hbar$ is the transition frequency. τ_1 and τ_2 are introduced phenomenologically in order to model the relaxation of occupations to quasiequilibrium and the dephasing of polarizations due to carrier-phonon and carrier-carrier scattering. In the numerical calculations, we use typical values of $\tau_1 = 120$ fs and $\tau_2 = 82.3$ fs [29,30]. $n_{\lambda\mathbf{k}_\parallel}^{\text{eq}}(n,T)$ is a quasiequilibrium thermal occupation at $T = 300$ K, which has the same carrier density $n(t)$ as the actual time-dependent occupation.

The exciting light field with a central frequency ω is given by

$$\mathbf{E}(t) = \mathbf{E}_\omega(t)e^{i\omega t} + \text{c.c.}, \quad (7)$$

where $\mathbf{E}_\omega$ is the slowly varying envelope function. To describe Gaussian-shaped pulses that propagate along the z direction, we use $\mathbf{E}_\omega$ in the form

$$\mathbf{E}_\omega(t) = E_0 e^{-\frac{t^2}{2\tau_L^2}}(\cos\theta, \sin\theta e^{i\phi}, 0), \quad (8)$$

where E_0 is the maximal amplitude, τ_L is the duration of the Gaussian envelope, θ is the polarization angle with respect to the x axis, and ϕ is the phase difference between the x and the y components of the field. If $\phi = \pm\pi/2$ and $\theta = \pi/4$, the light field is circularly polarized, whereas $\phi = 0$, which is used in all simulations presented below, corresponds to linearly polarized pulses. The vector potential used in the SBE (5) and (6) is given by $\mathbf{A}(t) = -\int_{-\infty}^{t} \mathbf{E}(t')dt'$.

By solving the SBE for an initially unexcited QW system, we obtain the time-dependent occupations $n_{\lambda\mathbf{k}_\parallel}$ and

microscopic polarizations $p_{\lambda\lambda'\mathbf{k}_\parallel}$. From the occupations, we can evaluate the intraband charge current known as injection photocurrent via

$$\mathbf{j}_{\text{inject}}(t) = e \sum_{\lambda,\mathbf{k}_\parallel} \mathbf{v}_{\lambda\lambda\mathbf{k}_\parallel} n_{\lambda\mathbf{k}_\parallel}$$

$$= e \sum_{c,\mathbf{k}_\parallel} \mathbf{v}_{cc\mathbf{k}_\parallel} n_{c\mathbf{k}_\parallel} + e \sum_{v,\mathbf{k}_\parallel} \mathbf{v}_{vv\mathbf{k}_\parallel} n_{v\mathbf{k}_\parallel}, \qquad (9)$$

where c (v) is a band index of the conduction (valence) band.

From the microscopic polarizations, it is possible to compute the charge current induced by interband and intersubband transitions,

$$\mathbf{j}_{\text{inter}}(t) = e \sum_{\lambda,\lambda'\neq\lambda,\mathbf{k}_\parallel} \mathbf{v}_{\lambda\lambda'\mathbf{k}_\parallel} p_{\lambda\lambda'\mathbf{k}_\parallel}$$

$$= e \sum_{c,c'\neq c,\mathbf{k}_\parallel} \mathbf{v}_{cc'\mathbf{k}_\parallel} p_{cc'\mathbf{k}_\parallel} + e \sum_{v,v'\neq v,\mathbf{k}_\parallel} \mathbf{v}_{vv'\mathbf{k}_\parallel} p_{vv'\mathbf{k}_\parallel}$$

$$+ e \sum_{c,v,\mathbf{k}_\parallel} (\mathbf{v}_{cv\mathbf{k}_\parallel} p_{cv\mathbf{k}_\parallel} + \text{c.c.}) \qquad (10)$$

as well as the interband and intersubband polarization,

$$\mathbf{P}_{\text{inter}}(t) = e \sum_{\lambda,\lambda'\neq\lambda,\mathbf{k}_\parallel} \mathbf{r}_{\lambda\lambda'\mathbf{k}_\parallel} p_{\lambda\lambda'\mathbf{k}_\parallel}$$

$$= e \sum_{c,c'\neq c,\mathbf{k}_\parallel} \mathbf{r}_{cc'\mathbf{k}_\parallel} p_{cc'\mathbf{k}_\parallel} + e \sum_{v,v'\neq v,\mathbf{k}_\parallel} \mathbf{r}_{vv'\mathbf{k}_\parallel} p_{vv'\mathbf{k}_\parallel}$$

$$+ e \sum_{c,v,\mathbf{k}_\parallel} (\mathbf{r}_{cv\mathbf{k}_\parallel} p_{cv\mathbf{k}_\parallel} + \text{c.c.}), \qquad (11)$$

where $e\mathbf{r}_{\lambda\lambda'\mathbf{k}_\parallel}$ is the transition dipole moment, which can be obtained from the velocity operator via the relation $\mathbf{v}_{\lambda\lambda'\mathbf{k}_\parallel} = i\omega_{\lambda\lambda'\mathbf{k}_\parallel} \mathbf{r}_{\lambda\lambda'\mathbf{k}_\parallel}$.

The shift current $\mathbf{j}_{\text{shift}}$ is defined as the zero-frequency contribution to the interband photocurrent $\mathbf{j}_{\text{inter}}$. Similarly, the optical rectification $\mathbf{P}_{\text{rect}}$ is given by the slowly varying part of the interband polarization $\mathbf{P}_{\text{inter}}$. The time derivative of the optical rectification provides the rectification current

$$\mathbf{j}_{\text{rect}}(t) = \frac{\partial}{\partial t} \mathbf{P}_{\text{rect}}(t). \qquad (12)$$

As explained in Sec. III in more detail, to obtain $\mathbf{j}_{\text{shift}}(t)$ and $\mathbf{j}_{\text{rect}}(t)$, we Fourier transform $\mathbf{j}_{\text{inter}}(t)$ and $\frac{\partial}{\partial t}\mathbf{P}_{\text{inter}}(t)$, respectively, into the frequency domain, apply a filter around $\omega = 0$, and transform back to the time domain.

In the limit of weak excitation intensities, the light-matter interaction can be considered as a perturbation. Using a second-order perturbation expansion of the SBE (5) and (6), by applying the rotating-wave approximation for the first-order microscopic polarization $p_{\lambda\lambda'}^{(1)}$, and neglecting 2ω terms in the second-order microscopic polarization $p_{\lambda\lambda'}^{(2)}$, we analytically derive approximate expressions for the injection current, the shift current, and the optical rectification, respectively, that

read [1,6]

$$\frac{\partial}{\partial t}\mathbf{j}_{\text{inject}}^{(2)} = \frac{2e^3}{\hbar^2\omega^2} \sum_{c,v,\mathbf{k}_\parallel} (\mathbf{v}_{cc\mathbf{k}_\parallel} - \mathbf{v}_{vv\mathbf{k}_\parallel})|\mathbf{E}_\omega \cdot \mathbf{v}_{cv\mathbf{k}_\parallel}|^2$$

$$\times \frac{1/\tau_2}{(\omega - \omega_{cv\mathbf{k}_\parallel})^2 + 1/\tau_2^2} - \mathbf{j}_{\text{inject}}^{(2)}/\tau_1, \qquad (13)$$

$$\mathbf{j}_{\text{shift}}^{(2)} = -\frac{2e^3}{\hbar^2\omega^2}\text{Im} \sum_{c,v,\mathbf{k}_\parallel} \frac{\mathbf{E}_\omega \cdot \mathbf{v}_{cv\mathbf{k}_\parallel}}{\omega - \omega_{cv\mathbf{k}_\parallel} + i/\tau_2}$$

$$\times \left[\sum_{\lambda\neq v} \mathbf{r}_{v\lambda\mathbf{k}_\parallel}(\mathbf{E}_\omega^* \cdot \mathbf{v}_{\lambda c\mathbf{k}_\parallel}) - \sum_{\lambda\neq c} (\mathbf{E}_\omega^* \cdot \mathbf{v}_{v\lambda\mathbf{k}_\parallel})\mathbf{r}_{\lambda c\mathbf{k}_\parallel} \right], \qquad (14)$$

and

$$\mathbf{P}_{\text{rect}}^{(2)} = \frac{2e^3}{\hbar^2\omega^2}\text{Re} \sum_{c,v,\mathbf{k}_\parallel} \frac{\mathbf{E}_\omega \cdot \mathbf{v}_{cv\mathbf{k}_\parallel}}{\omega - \omega_{cv\mathbf{k}_\parallel} + i/\tau_2}$$

$$\times \left[\sum_{\lambda\neq v} \frac{\mathbf{r}_{v\lambda\mathbf{k}_\parallel}}{\omega_{v\lambda\mathbf{k}_\parallel}}(\mathbf{E}_\omega^* \cdot \mathbf{v}_{\lambda c\mathbf{k}_\parallel}) - \sum_{\lambda\neq c} (\mathbf{E}_\omega^* \cdot \mathbf{v}_{v\lambda\mathbf{k}_\parallel})\frac{\mathbf{r}_{\lambda c\mathbf{k}_\parallel}}{\omega_{\lambda c\mathbf{k}_\parallel}} \right]. \qquad (15)$$

III. NUMERICAL RESULTS

In this section, we present and discuss results obtained from numerical solutions of the SBE for GaAs/Al$_{0.35}$Ga$_{0.65}$As QWs grown in the crystallographic [110] and [111] directions. The band parameters for GaAs and Al$_x$Ga$_{1-x}$As are taken from Ref. [26], and the temperature dependence of the band gap is described by the Varshni relation. In our calculations, we consider room temperature ($T = 300$ K). For the optical excitation, we use linearly polarized laser pulses that propagate perpendicular to the QW plane, i.e., in the z direction, and have a Gaussian envelope with a duration of $\tau_L = 150$ fs. The geometry of the excitation is illustrated in Fig. 1.

The band structure of the QW system is obtained from a matrix diagonalization using $14\,N$ bands, where we use $N \geqslant 20$. Due to this large number of bands, the direct evaluation of the multisubband SBE (6) and (5) beyond the rotating-wave approximation is numerically very intensive. To keep the calculation feasible, we limit the number of bands included in the numerics to 40. In particular, we take into account the 18 energetically highest valence subbands, six energetically lowest s-like conduction subbands, and 16 energetically lowest p-like conduction subbands. Although the optical excitation to p-like conduction bands is nonresonant, the presence of these bands in the SBE is necessary. In second-order processes, the p-like conduction-band states play the role of intermediate states for the transition of electrons from the valence to the conduction band and thereby contribute to the shift and rectification currents.

Obtaining shift and rectification currents from numerical solutions of the SBE involves basically the following steps: (i) solve the SBE, (ii) compute the current $\mathbf{j}_{\text{inter}}(t)$ and the interband polarization $\mathbf{P}_{\text{inter}}(t)$, (iii) Fourier transform $\mathbf{j}_{\text{inter}}(t)$ and $\mathbf{P}_{\text{inter}}(t)$ to the frequency domain and apply a frequency
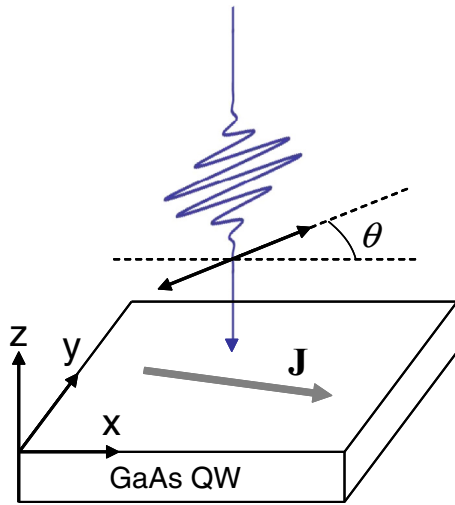
FIG. 1. Schematic illustration of the shift and rectification current generation using linearly polarized light pulses. θ is the light polarization angle with respect to the x axis.

filter to remove the high-frequency components, and (iv) inversely Fourier transform back to the time domain to obtain the shift current $\mathbf{j}_{\text{shift}}(t)$ and the optical rectification $\mathbf{P}_{\text{rect}}(t)$. We carefully checked the convergence versus the number of bands, and we compared the complete numerical solutions with the analytical second-order approximation, i.e., Eqs. (14) and (15), where we included all 14 N bands to ensure that our approach

works properly within excitation conditions considered in the paper.

A. [110]-oriented quantum wells

We consider a GaAs QW of 10 nm width grown along the [110] crystallographic direction using a coordinate system in which $x = [001]$, $y = [1\bar{1}0]$, and $z = [110]$. In the following, we analyze shift and rectification currents generated by linearly polarized laser pulses. The laser field has a photon energy of 1.54 eV, i.e., 80 meV above the band gap ($E_g = 1.46$ eV). For light polarization along the y axis, we obtain the current flowing in the x direction, named xyy current. The computed time evolution of xyy shift and rectification current densities in the GaAs QW for different laser amplitudes is displayed in Figs. 2(a)–2(c) and Figs. 2(d) and 2(e), respectively. Here, solid (dashed) lines correspond to a nonperturbative complete (perturbative second-order) solution of the SBE. When the amplitude of the light field is small, the perturbative approximation agrees well with the nonperturbative complete solution; see Figs. 2(a) and 2(d) for $E_0 = 10^4$ V/cm. In this perturbative regime, the shift current follows the envelope of optical pulse intensity while the rectification current has the shape of its time derivative. The small difference between the two approaches is due to contributions from heavy- to light-hole transitions, which are enabled by the finite bandwidth of the incident pulse and can only be described in the nonperturbative solution. When the light-field amplitude is large enough such that band-filling effects become
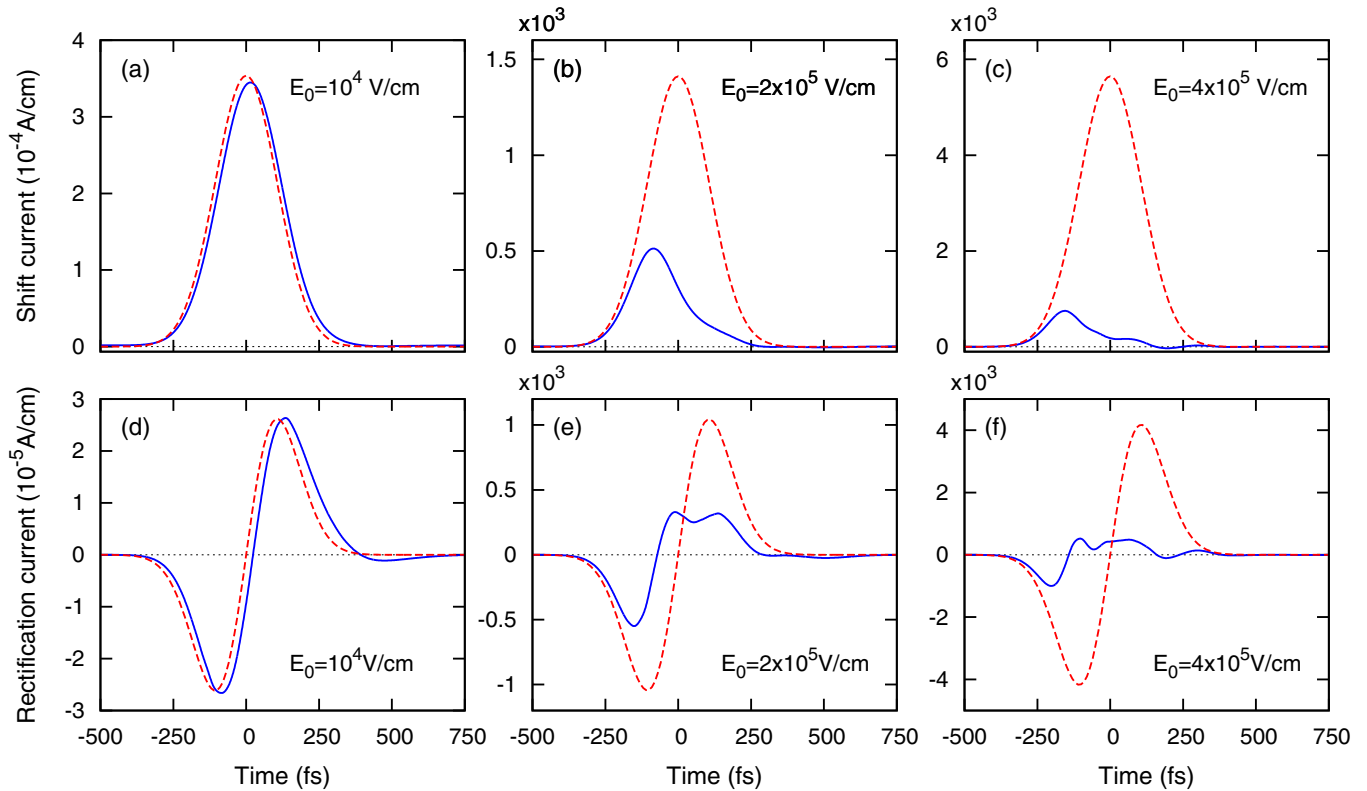
FIG. 2. Dynamics of shift and rectification currents in a 10-nm-wide [110]-oriented GaAs QW for different peak amplitudes of the laser pulses. The dashed lines are obtained by a perturbative second-order analysis of the light-matter interaction, whereas the solid lines are obtained by solving the full SBE.

relevant, there are strong deviations between the approximate perturbative and the full nonperturbative results; see Figs. 2(b) and 2(e) for $E_0 = 2 \times 10^5$ V/cm, and Figs. 2(c) and 2(f) for $E_0 = 4 \times 10^5$ V/cm. In this regime, the second-order approximation fails to describe the shift current dynamics properly, and it strongly overestimates the current magnitude. In particular, the nonperturbative solutions of the SBE result in significantly smaller currents since phase-space filling limits the strengths of the optical excitations, and due to Rabi flopping in the strongly excited regions of k space an oscillatory dynamics is obtained; see the solid lines in Figs. 2(b), 2(c), 2(e), and 2(f).

For bulk GaAs, the relevance of phase-space filling effects in limiting the perturbative (in this case) $\chi^{(3)}$ scaling of two-color injection currents has been confirmed recently [31], and it can therefore be expected that also for shift and rectification currents, nonperturbative signatures should be observable. However, for the excitation with one-color optical laser pulses, the third-order response is oscillating rapidly with optical frequencies, and therefore in $\chi^{(3)}$ no contribution to low-frequency shift and rectification currents is expected [32]. Thus for shift and rectifications currents, $\chi^{(4)}$ represents the lowest-order correction to the low-intensity second-order $\chi^{(2)}$ scaling. Whereas limiting our calculations to fourth order would result in a single direction reversal of the currents, such an approximation would also lead to an unphysical scaling of the currents with the fourth power of the electric field amplitude for high fields, as nonperturbative effects such as Rabi flopping, which limit the strength of the currents, are not included.

In the following, we focus on the weak-excitation regime ($E_0 = 10^4$ V/cm) where the perturbative second-order solution works properly, and we analyze the dependence of shift and rectification currents on the other excitation conditions, in particular the light polarization and the photon energy. In Fig. 3 we show the x and y components of the peak value of shift current density [Fig. 3(a)] and rectification current density [Fig. 3(b)] as functions of θ, where θ is measured with respect to the $x = [001]$ direction and determines the polarization direction of the linearly polarized incident pulse. The computed current components are well described by a formula that also arises from a macroscopic symmetry analysis: $j_x = A + B \cos 2\theta$ and $j_y = C \sin 2\theta$ [16,17]. We note that for light polarization parallel to the x axis ($\theta = 0°$), there is a finite current flowing in the x direction, i.e., xxx current. This kind of current is not present in bulk GaAs, but it does exist in [110]-oriented GaAs QWs because of the symmetry reduction.

The peak value of the xyy (xxx) shift current density versus the photon energy is presented by the black solid line in Fig. 4 for $\theta = 90°$ ($\theta = 0°$), i.e., the polarization of the incident field is in the y direction (x direction). Upon increasing the photon energy near and above the band gap, both xyy and xxx shift currents show a nonmonotonic and complex variation. The xxx current shows a very interesting sign change that corresponds to a reversal of the current direction at the photon energy of 1.504 eV; see the solid line in Fig. 4(b). To understand the origin of the complex dependence of shift currents, we calculate separately three different contributions to the net current according to Eq. (10).
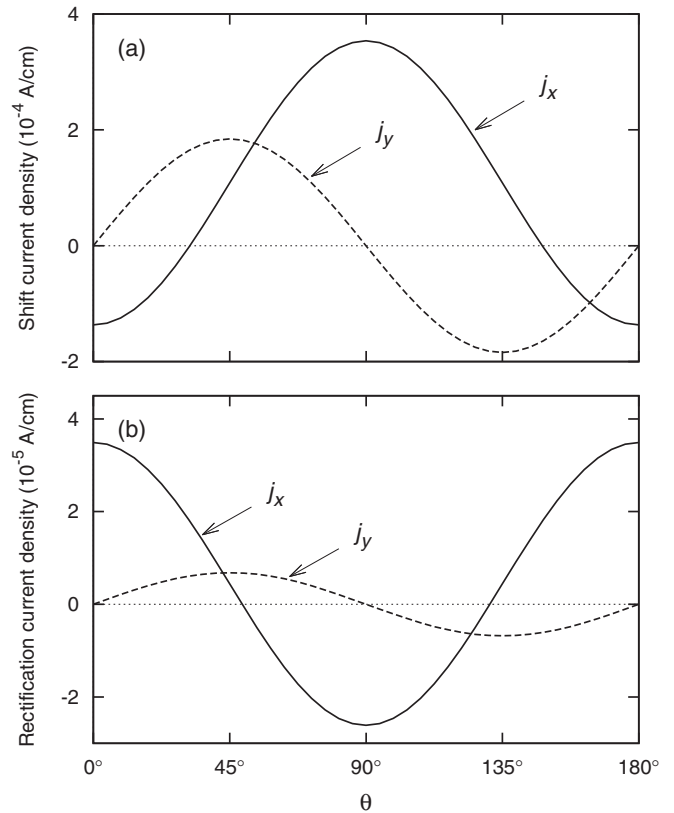
FIG. 3. Components in the x and y directions of the peak value of shift (a) and rectification (b) current densities as a function of the light polarization angle θ in a 10 nm [110]-oriented GaAs QW.

Currents originating from inter-conduction-band polarizations $p_{cc'}$ ($j_{cc'}$), inter-valence-band polarizations $p_{vv'}$ ($j_{vv'}$), and interband polarizations p_{cv} (j_{cv}) are evaluated separately and plotted as dotted, dashed, and dash-dotted lines, respectively. Since $j_{cc'}$ and j_{cv} shown in Fig. 4(a) follow the steplike increase of the two-dimensional interband density of states, the strong variation of $j_{vv'}$ in both magnitude and direction is responsible for the nonmonotonic photon-energy dependence of the net xyy shift current. In the case of the xxx current, because of very small contributions of $j_{cc'}$ and j_{cv}, the net shift current is mainly given by $j_{vv'}$. To obtain nonvanishing $j_{vv'}$, it is necessary that velocity matrix elements $\mathbf{v}_{cv}$, $\mathbf{v}_{cv'}$, and $\mathbf{v}_{vv'}$ are simultaneously nonvanishing. At $\mathbf{k}_\parallel \neq \mathbf{0}$, heavy- and light-hole states are mixed, which allows the velocity matrix elements between all pairs of c, v, and v' subbands to have finite and k-dependent values. If we artificially remove the valence-band mixing by setting the coupling matrix elements between heavy and light holes to zero, the contribution $j_{vv'}$ vanishes and we obtain a monotonically increasing xyy shift current and a negligibly small xxx shift current, shown as red solid lines in Figs. 4(a) and 4(b), respectively.

The photon-energy dependence of xyy and xxx rectification currents is presented in Fig. 5, showing also a complex, oscillatory variation. Using the same analysis as for shift currents, we find that the dominant contribution to both the xyy and xxx rectification currents comes from inter-valence-band polarizations, i.e., $j_{vv'}$. The photon-energy
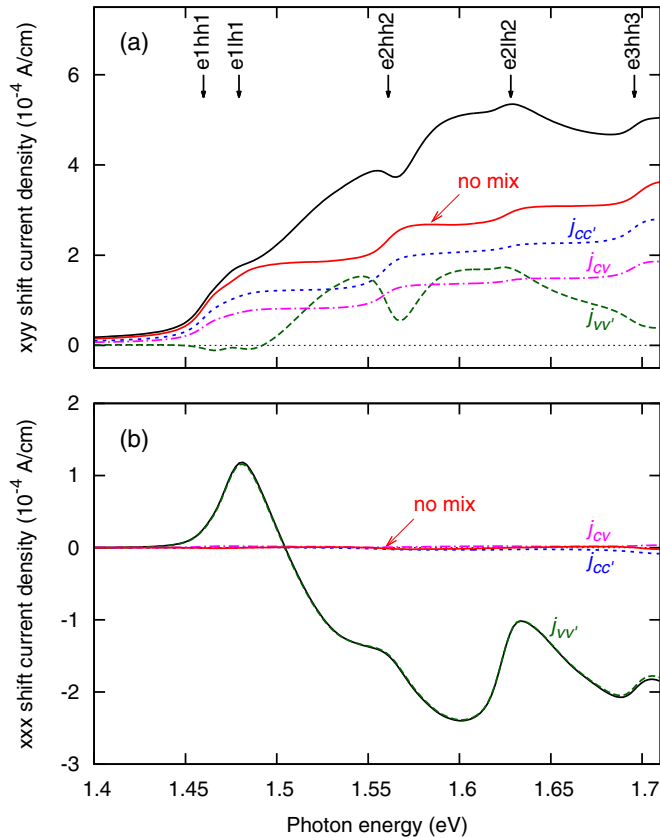
FIG. 4. Peak values of the xyy (a) and xxx (b) shift current densities vs photon energy for a 10-nm-wide [110]-oriented GaAs QW. Black solid line: total shift current. Blue dotted line: inter-conduction-band contribution $j_{cc'}$. Green dashed line: inter-valence-band contribution $j_{vv'}$. Magenta dash-dotted line: interband contribution j_{cv}. Red solid line: without heavy-hole–light-hole coupling. The vertical arrows highlight the photon energies corresponding to interband transitions at $\mathbf{k}_\parallel = \mathbf{0}$.

dependence of rectification current is therefore governed by valence-band mixing. Furthermore, the sign change of the optical rectification at the resonance excitation [see Eq. (15) for $\omega = \omega_{cv\mathbf{k}_\parallel}$] may lead to a direction reversal of the rectification current with increasing photon energy [3,15].

B. [111]-oriented quantum wells

For [111]-oriented QWs, a coordinate system of $x = [11\bar{2}]$, $y = [\bar{1}10]$, and $z = [111]$ is chosen. We compute the photocurrents in a 10-nm-wide GaAs QW using an incident pulse with a peak amplitude of $E_0 = 10^4$ V/cm. Figure 6 shows the x and y components of shift and rectification current densities versus the polarization angle θ for a photon energy of 1.52 eV. The calculated data are fitted well by the formulas $j_x = A\cos 2\theta$ and $j_y = -A\sin 2\theta$. The polarization-direction dependence of the shift and rectification currents in [111]-oriented QW is quite similar to [111]-oriented bulk GaAs [3].

The photon-energy dependence of the shift and the rectification current densities is shown in Fig. 7 for the light polarization parallel to the $y = [\bar{1}10]$ direction ($\theta = 90°$). Similarly to the case of [110]-oriented QWs, also for [111]-oriented QWs a complex and nonmonotonic dependence of
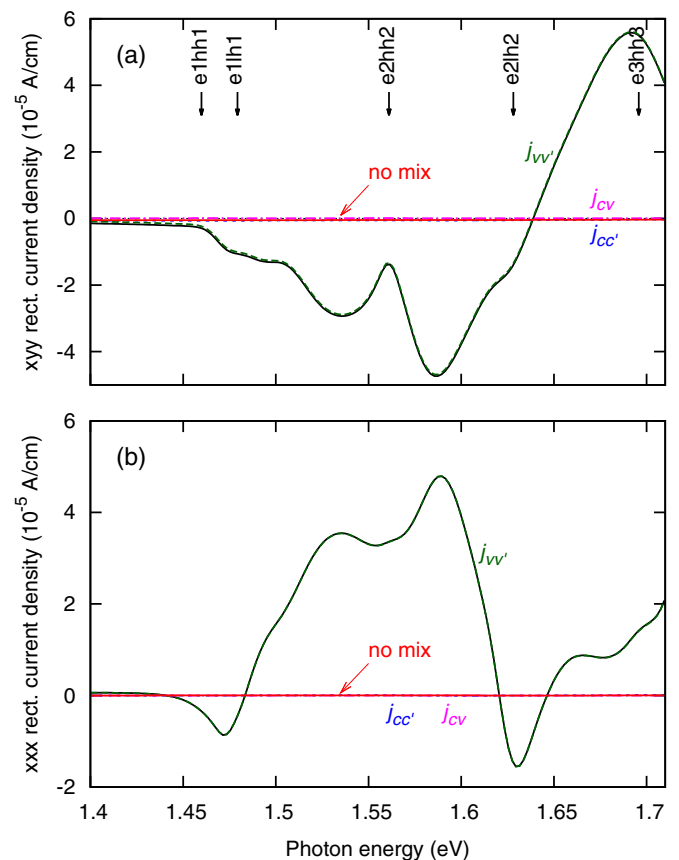
FIG. 5. Peak values of the xyy (a) and xxx (b) rectification current densities vs the photon energy for a 10-nm-wide [110]-oriented GaAs QW. The description of the lines is the same as in Fig. 4.

the shift and the rectification currents on photon energy is obtained.

IV. COMPARISON TO EXPERIMENTS

Since the shift current involves real carriers, its amplitude is typically much larger than the rectification current amplitude under the same excitation conditions; see also Figs. 4, 5, and 7. Therefore, for an analysis of the experiments, we only consider shift currents and neglect rectification currents. A comparison between experiments and simulations on injection currents is given in Ref. [19].

For the shift current experiments, we employed a standard free-space terahertz (THz) setup in transmission geometry [16,17,33]. The samples consist of [110]-oriented GaAs QWs with well widths of 12, 15, and 20 nm. They were excited at normal incidence with a 150 fs laser pulse originating from a Ti:sapphire oscillator with a repetition rate of 76 MHz. The optical peak intensity in front of the samples was 60 MW/cm^2, resulting in two-dimensional carrier densities of approximately 2×10^{11} cm^{-2}. The center photon energy of the femtosecond laser could be varied, allowing for different excitation conditions. The polarization of the initially linearly polarized pump beam was aligned to the x direction of the samples.
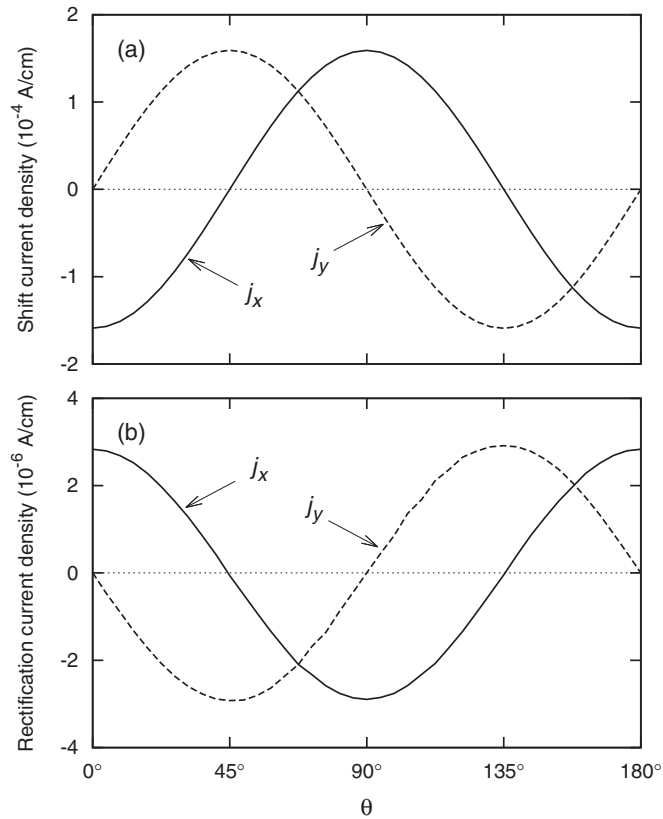
FIG. 6. Peak value of shift (a) and rectification (b) current densities in the x and y directions as a function of the light polarization angle θ in a 10-nm-wide [111]-oriented GaAs QW.

FIG. 7. Peak value of shift (a) and rectification (b) current densities as a function of photon energy in a 10-nm-wide [111]-oriented GaAs QW. Vertical arrows show the photon energies corresponding to interband transitions at $\mathbf{k}_{\parallel} = \mathbf{0}$.

After generation, the shift currents decay on a femtosecond time scale. Since the emitted electromagnetic radiation is proportional to the time derivative of the current transients, THz radiation is emitted. The THz radiation was collected from the samples' backsurface with an off-axis parabolic mirror, guided to a second off-axis parabolic mirror, and focused down onto 1-mm-thick [110]-oriented ZnTe crystal. The probe pulse was guided through a small hole in the second off-axis parabolic mirror and collinearly overlapped with the THz pulse to read out the electric field-induced refractive index change of the electro-optic crystal. A silicon wafer and a THz polarizer were placed between the two off-axis parabolic mirrors. The silicon wafer blocked any scattered pump light. The THz polarizer allowed us to detect currents flowing in certain directions in the sample since the polarization of the THz radiation in the far field is parallel to the direction of the current flow. This is a large advantage of THz experiments over experiments based on charge collection at electrodes, since the THz setup is only sensitive to currents flowing in the plane of the sample. In the experiments, the THz polarizer was oriented such that only shift currents flowing along the x direction were detected. The bandwidth of the experimental setup was limited by the velocity mismatch between the group velocity of the optical pulse and the phase velocity of the THz pulse in the electro-optic crystal. These restrictions allowed for the detection of frequencies up to approximately 3 THz. All experiments were done at room temperature.

In Fig. 8, we plot the THz amplitude emitted from the xxx shift currents in the three QW samples versus excitation photon energy. Additionally, the calculated peak magnitude of the xxx shift current is shown. Starting with the 20 nm QW, we obtain an excellent agreement between theory and experiment in nearly the complete photon energy range. In particular, the peaks at 1.5 and 1.57 eV and also a zero crossing at 1.45 eV are nicely reproduced. The deviations between experiment and theory at small photon energy are most likely because we neglect the Coulomb interaction in the simulations. As was shown in Ref. [20] for the case of injection currents, we expect also for shift currents that excitonic effects originating from the electron-hole attraction will mainly increase the strength of the current response near the band gap and lead to a spectral shift to lower energies due to the excitonic binding energy. Thus including excitonic effects in our simulations should further improve the agreement between experiment and theory at small photon energies. The deviations in Fig. 8 at large photon energies might be the result of improper rescaling of the measured signals. At these photon energies, the optical pump and probe power decreased due to the end of the tuning range of our femtosecond laser.

The deviations between experiment and theory at small and large photon energies also appear for the 15 and 12 nm QWs; otherwise, the overall agreement between experiment and theory is also good for these QW samples. In general,
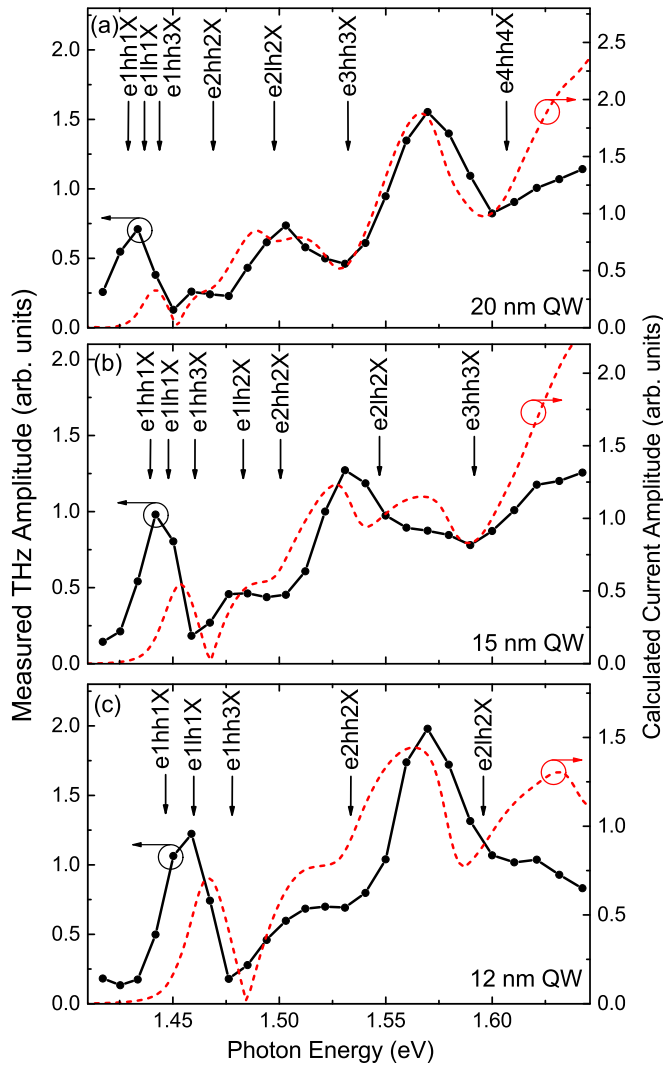
FIG. 8. Measured THz amplitudes emitted from shift currents (solid black) and calculated absolute peak values of shift currents (dashed red) in the x direction in [110]-oriented GaAs QWs of different well width: (a) 20 nm, (b) 15 nm, and (c) 12 nm.

(ii) it confirms that the measured signal is mainly caused by the shift of the electron charge during excitation and not by scattering contributions [2].

V. CONCLUSIONS

We present a unified microscopic approach that is capable of describing fully dynamically all three kinds of single-frequency photocurrents in noncentrosymmetric semiconductor QWs, i.e., injection, shift, and rectification currents. Our approach has been applied to analyze shift and rectification currents generated by linearly polarized incident pulses in [110]- and [111]-oriented GaAs/AlGaAs QWs.

The dependence of the photocurrents on the polarization direction of the incident laser pulses has been studied. For shift and rectification currents, we compared the nonperturbative solution of the SBE to a second-order approximation. It is demonstrated that intrinsic nonlinearities arising from phase-space filling effects and Rabi flopping, which are not included in the second-order approximation, lead to a significant difference between the two solutions in the limit of strong excitation intensities ($E_0 > 10^5$ V/cm).

Unlike optical interband absorption, which increases in steps with increasing photon energy, we find an unexpected complex and nonmonotonic dependence of shift and rectification currents on the photon energy in both theory and experiments. In certain spectral regions, both currents may even change their direction. It has been demonstrated that this dependence is the result of band mixing of the heavy- and light-hole valence bands. This excitation frequency dependence of the photocurrents might be employed for new applications such as optoelectronic converters or modulators.

ACKNOWLEDGMENTS

the good agreement between experiment and theory is very important, since (i) it validates the theoretical approach, and

[1] V. I. Belinicher, E. L. Ivchenko, and B. I. Sturman, Sov. Phys. JETP **56**, 359 (1982).

[2] B. I. Sturman and V. M. Fridkin, *The Photovoltaic and Photorefractive Effects in Noncentrosymmetric Materials* (Gordon and Breach, Philadelphia, 1992).

[3] X.-C. Zhang, Y. Jin, K. Yang, and L. J. Schowalter, Phys. Rev. Lett. **69**, 2303 (1992).

[4] J. B. Khurgin, J. Opt. Soc. Am. B **13**, 2129 (1996).

[5] P. Král, J. Phys.: Condens. Matter **12**, 4851 (2000).

[6] J. E. Sipe and A. I. Shkrebtii, Phys. Rev. B **61**, 5337 (2000).

[7] R. D. R. Bhat and J. E. Sipe, Phys. Rev. Lett. **85**, 5432 (2000).

[8] S. D. Ganichev, E. L. Ivchenko, S. N. Danilov, J. Eroms, W. Wegscheider, D. Weiss, and W. Prettl, Phys. Rev. Lett. **86**, 4358 (2001).

[9] S. D. Ganichev, U. Rössler, W. Prettl, E. L. Ivchenko, V. V. Belkov, R. Neumann, K. Brunner, and G. Abstreiter, Phys. Rev. B **66**, 075328 (2002).

[10] L. E. Golub, Phys. Rev. B **67**, 235320 (2003).

[11] D. Côté, N. Laman, and H. M. van Driel, Appl. Phys. Lett. **80**, 905 (2002).

[12] N. Laman, M. Bieler, and H. M. van Driel, J. Appl. Phys. **98**, 103507 (2005).

[13] M. Bieler, K. Pierz, U. Siegner, and P. Dawson, Phys. Rev. B **73**, 241312(R) (2006).

[14] R. D. R. Bhat, F. Nastos, A. Najmaie, and J. E. Sipe, Phys. Rev. Lett. **94**, 096603 (2005).

[15] F. Nastos and J. E. Sipe, Phys. Rev. B **74**, 035201 (2006).

[16] M. Bieler, K. Pierz, and U. Siegner, J. Appl. Phys. **100**, 083710 (2006).

[17] M. Bieler, K. Pierz, U. Siegner, and P. Dawson, Phys. Rev. B **76**, 161304(R) (2007).

[18] J. M. Schleicher, S. M. Harrel, and C. A. Schmuttenmaer, J. Appl. Phys. **105**, 113116 (2009).

[19] S. Priyadarshi, A. M. Racu, K. Pierz, U. Siegner, M. Bieler, H. T. Duc, J. Förstner, and T. Meier, Phys. Rev. Lett. **104**, 217401 (2010).

[20] H. T. Duc, J. Förstner, and T. Meier, Phys. Rev. B **82**, 115316 (2010).

[21] F. Nastos and J. E. Sipe, Phys. Rev. B **82**, 235204 (2010).

[22] J. E. Moore and J. Orenstein, Phys. Rev. Lett. **105**, 026805 (2010).

[23] J. W. McIver, D. Hsieh, H. Steinberg, P. Jarillo-Herrero, and N. Gedik, Nat. Nanotech. **7**, 96 (2012).

[24] D. A. Bas, K. Vargas-Velez, S. Babakiray, T. A. Johnson, P. Borisov, T. D. Stanescu, D. Lederman, and A. D. Bristow, Appl. Phys. Lett. **106**, 41109 (2015).

[25] U. Rössler, Solid State Commun. **49**, 943 (1984).

[26] R. Winkler, *Spin-orbit Coupling Effects in Two-Dimensional Electron and Hole Systems* (Springer, Berlin, 2003).

[27] M. El kurdi, G. Fishman, S. Sauvage, and P. Boucaud, Phys. Rev. B **68**, 165333 (2003).

[28] H. Haug and S. W. Koch, *Quantum Theory of the Optical and Electronic Properties of Semiconductors*, 4th ed. (World Scientific, Singapore, 2004).

[29] B. Pasenow, H. T. Duc, T. Meier, and S. W. Koch, Solid State Commun. **145**, 61 (2008).

[30] H. T. Duc, T. Meier, and S. W. Koch, Phys. Rev. Lett. **95**, 086606 (2005).

[31] E. Sternemann, T. Jostmeier, C. Ruppert, H. T. Duc, T. Meier, and M. Betz, Phys. Rev. B **88**, 165204 (2013).

[32] C. Aversa and J. E. Sipe, Phys. Rev. B **52**, 14636 (1995).

[33] M. Bieler, IEEE J. Sel. Top. Quantum Electron. **14**, 458 (2008).